Vibrational, electronic, and vibronic excitations of polar $C_{60}F_{18}$ molecules: Experimental and theoretical study

A. A. Popov, V. M. Senyavin, V. I. Korepanov, and I. V. Goldt
Department of Chemistry, Moscow State University, 119992 Moscow, Russia

A. M. Lebedev, V. G. Stankevich, K. A. Menshikov, and N. Yu. Svechnikov
Russian Research Centre Kurchatov Institute, 123182 Moscow, Russia

O. V. Boltalina
Department of Chemistry, Colorado State University, Fort Collins, Colorado 80523, USA

I. E. Kareev
Institute of Problems of Chemical Physics, Russian Academy of Sciences, Chernogolovka 142432, Russia

S. Kimura and O. Sidorova
UVSOR Facility, Institute of Molecular Science, Okazaki 444-8585, Japan

K. Kanno and I. Akimoto
Department of Material Science and Chemistry, Wakayama University, 930 Sakaedani, Wakayama 640-8510, Japan
(Received 26 August 2008; published 15 January 2009)

Polarized optical conductivity spectra in the IR and visible range and variable-temperature photoluminescence spectra of the $C_{60}F_{18}$ single crystals in the 4–300 K temperature range are reported. Density-functional theory (DFT) calculations of vibrational spectra and time-dependent DFT calculations of the excitation energies of the $C_{60}F_{18}$ molecule are performed to interpret experimentally observed phenomena. Orientation of the C_{3v}-symmetric $C_{60}F_{18}$ molecules in the single crystal is revealed by comparison of the experimental polarized IR spectra and vibrational DFT calculations. A_2 symmetry is assigned to the lowest energy singlet excited state of $C_{60}F_{18}$, and hence pure electronic $S_0 \rightarrow S_1$ excitation is found to be dipole forbidden. Fine vibronic structure found at low temperature is interpreted in terms of Herzberg-Teller and Franck-Condon mechanisms. Considerable similarity with vibronic spectra of C_{60} is found and explained by presumable localization of the lowest energy electronic excitation of $C_{60}F_{18}$ on the fullerenelike part of the molecule.

DOI: 10.1103/PhysRevB.79.045413 PACS number(s): 78.20.Bh, 78.30.Na, 78.40.Ri, 78.55.Kz

I. INTRODUCTION

Fullerenes and other carbon nanostructures remain in the focus of current research activity due to their unique structures and unusual fundamental physical properties, also growing interest in the practical applications in various areas is well documented.[1,2] One of the attractive features in the fullerene research is the possibility to modify carbon cages of fullerenes so that their properties can be tuned in a controlled manner. For example, substitutional doping approach may allow tuning of optical gaps of fullerene derivatives from the near infrared up to the ultraviolet.[3] This type of doping involves substitution of one or more C atoms in the cage with heteroatom, and known examples from experiment include azafullerenes[4] and $C_{58}BN$.[5]

Exohedral derivatization of fullerenes is more common and more extensively developed type of chemical modification, and possibilities for obtaining functionalized fullerenes with tunable optical gaps have recently been explored.[6] Among the products of polyadditions to fullerenes, fluorine-containing derivatives stand out due to the their highly enhanced electron-accepting properties ($C_{60}F_{48}$ has a record-high electron affinity of 4 eV among fluoro-organic compounds[7]), high thermal stability, and wide range of available compositions and diversity of molecular structures.[8]

Spectroscopic and theoretical studies of fluorinated fullerenes have been published since early 1990s when the first samples of fluorinated C_{60} were prepared, but this early work was complicated due to the fact that fluorofullerenes formed in those reactions represented mixtures of compounds, which compositions and structures were not known. Only in the last decade, progress in selective fluorination techniques with the use of F_2 (Refs. 9 and 10) or metal fluorides[11] resulted in the preparation and structural characterization of several fluorofullerenes which represent single isomers.

$C_{60}F_{18}$ is one of the three fluorofullerenes that was obtained with high yield and purity (two others are $C_{60}F_{36}$ and $C_{60}F_{48}$). In the latter two compounds F atoms are distributed evenly on the fullerene cage, transforming conjugated π system of underivatized C_{60} into the structures with only few remaining isolated fragments of π system, either as isolated double bonds (as in $C_{60}F_{48}$) or benzenoid fragments (as in $C_{60}F_{36}$). In contrast, $C_{60}F_{18}$ has a structure which contains half of the carbon cage retaining conjugated π system of the fullerene and half of the molecule with attached 18 F atoms forming an isolated benzene ring on the pole [Fig. 1(a)]. Such a peculiar molecular structure originally was proposed on the basis of ^{19}F NMR spectroscopy,[12] and now is known

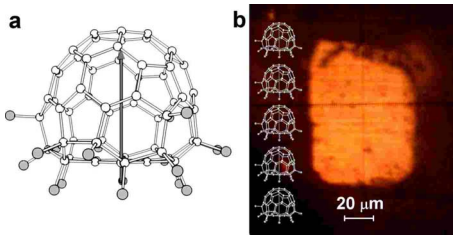

FIG. 1. (Color online) (a) Molecule of $C_{60}F_{18}$ showing direction of the dipolar moment; (b) photo of the crystal face used in the polarized spectroscopic measurements; one of the possible orientations of individual $C_{60}F_{18}$ molecules with respect to the crystal face is shown in (b) (opposite direction of dipolar moment is also possible; these two direction are indistinguishable with current experimental data).

with high precision from the single-crystal x-ray diffraction studies.[13–15]

As a result, $C_{60}F_{18}$ has very different properties from other polyfluorinated C_{60} compounds. For example, the dipole moment of $C_{60}F_{36}$ is close to zero, while $C_{60}F_{18}$ is estimated to have a large dipole moment of 10–12 D due to compact arrangement of fluorine atoms on one pole of the carbon sphere.[13] Electronic structures of $C_{60}F_{48}$ (Ref. 16) and to a lesser extent $C_{60}F_{36}$ (Ref. 17) have been studied both theoretically and experimentally, which demonstrated that these highly fluorinated fullerenes exhibit electronic properties typical for dielectrics with the large band gap.

In this work, we performed selected experimental spectroscopic studies on the high-purity samples of $C_{60}F_{18}$, including solvent-free single crystals grown via gas phase. Combination of the extensive theoretical calculations of the vibrational and excitation spectra with the experimental results obtained in this work and reported in the literature[18–22] allowed to propose in-depth interpretation and theoretical understanding of electronic structure of this fascinating molecule.

II. EXPERIMENTAL DETAILS

A crude sample of $C_{60}F_{18}$ was prepared in a reaction between C_{60} and K_2PtF_6 taken in 1:4 molar ratio at 450 °C for 6 h under dynamic vacuum. Details of the reaction conditions can be found in Ref. 14 The sublimed crude material contained $C_{60}F_{18}$ as a main product and some other fluorides $C_{60}F_n$ ($n=2-8,20,36$). A two-stage chromatographic procedure was used for isolation of the pure $C_{60}F_{18}$ sample. At the first separation stage, a Cosmosil Buckyprep column (20 mm i.d. $\times$ 250 mm, Nacalai Tesque, Inc.) (1.8 ml injections, 18 ml/min flow rate, toluene eluent) was used, affording initial isolation of the main fraction eluting between 35 and 40 min. This fraction was further processed using a second HPLC purification stage on a Regis BuckyClutcher column (20 mm i.d. $\times$ 250 mm, Regis Chemical Co.; 0.6 ml injections, 12 ml/min flow rate, toluene eluent). As a result, a very high-purity sample of $C_{60}F_{18}$ was prepared, and 99%+ purity was confirmed by HPLC, mass spectrometry, and ^{19}F NMR analyses. HPLC solvent (toluene) was evaporated to dryness in vacuum. Another sample of $C_{60}F_{18}$, a solvent-free single crystal, was also used in this work. This sample was prepared during the reaction between C_{60} and K_2PtF_6 under the conditions analogous to those described above. A solid sublimed material deposited on the coldest part of the glass reactor was carefully removed from the surface. Analysis by mass spectrometry, HPLC, and microscopy revealed that this material represented an aggregation of brownish-yellow rectangular plates—single crystals of $C_{60}F_{18}$ of very high purity, so the HPLC purification was not necessary for this sample. X-ray diffraction analysis of the single crystal at $T=180$ K gave the following cell parameters: monoclinic, space group C_C, $z=4$, $a=19.577(14)$ Å, $b=11.008(7)$ Å, $c=19.315(20)$ Å, $\alpha=\gamma=90°$, $\beta=120.917(6)°$, $V=3571(5)$ Å^3. These values are very close to the data obtained in our earlier crystallographic work on the solvent-free single crystal of $C_{60}F_{18}$,[14] allowing a suggestion on the close similarity of the molecular packing to be made. The single crystal chosen for the spectroscopic measurements had a rectangular shape with the size of rectangular planes of 60 $\times$ 100 μm^2 [Fig. 1(b)].

IR spectra of the powder samples of the HPLC-purified $C_{60}F_{18}$ were measured on the Equinox 55S Fourier-transform spectrometer (Bruker, Germany). Raman spectra were measured with the use of FT-Raman module FRA106 attached to Equinox 55. The spectra were excited by 1064 nm line of Nd doped yttrium aluminum garnet laser (laser power 150 mW, 200 scans, resolution 1 cm^{-1}). Absorption spectra were measured on the Specord-200 spectrophotometer (Analytik Jena, Germany) under resolution 1 nm. Photoluminescence (PL) spectra of $C_{60}F_{18}$ in toluene solution were measured on Shimadzu RF-5301PC Spectrofluorometer (resolution 3 nm, excitation in the visible and near UV range).

Fourier transform infrared Nicolet Magna 760 (600–12 000 cm^{-1}) and multichannel detection system Atago Macs 320 (11 000–33 000 cm^{-1}) combined with an IR microscope were used for reflectivity measurements in IR and visible (Vis hereafter) ranges. These measurements were carried out with two polarizations of the incoming radiation with respect to the long edge of the crystal plane. The crystal was mounted on the goniometric head and could be rotated relative to the orientation of a polarization vector of the incoming radiation so that parallel and perpendicular to the long side of the crystal orientations could be realized.

Variable temperature luminescence spectra of the crystalline $C_{60}F_{18}$ were measured with the use of microscopic detecting system in Wakayama University (Japan). The measurements were performed with the spatial resolution of ~5 μm and He–Cd laser excitation (325 nm).

III. COMPUTATIONAL DETAILS

All density-functional theory (DFT) (for ground state) and time-dependent (TD) DFT (for excited states) calculations were performed using PRIRODA program[23,24] employing Perdew-Burke-Ernzerhof (PBE) functional[25] and implemented triple-zeta basis set with two sets of polarization *d* functions (i.e., TZ2P-quality basis set). The quantum-chemical code employed expansion of the electron density in

an auxiliary basis set to accelerate evaluation of the Coulomb and exchange-correlation terms.[23] Raman intensities were computed numerically using PC GAMESS (Ref. 26) at the PBE0 level with 6–31G basis set. Our previous vibrational DFT studies of $C_{60}F_{20}$,[27] $C_{60}F_{36}$,[28] and $C_{60}F_{48}$ (Ref. 28) revealed that PBE/TZ2P approach reliably predicts force constants of the carbon cage, while the force constants of the stretching and bending C–F coordinates are systematically underestimated. Hence, DFT-computed force constant matrix of $C_{60}F_{18}$ was transferred into an internal coordinate system including all covalent bonds and valence angles and then scaled using Pulay procedure[29] so that the force constants of the carbon cage were kept unchanged, while for the stretching and bending C–F coordinates the scaling factors optimized for $C_{60}F_{20}$ (Ref. 27) were used (see Refs. 27 and 28 for further details of the scaling procedure).

Herzberg-Teller (HT) vibronic intensity of ith normal mode in the jth excited state was modeled by the numeric differentiation of the transition dipolar moment, i.e., distorting molecule along $\mathbf{L_i}$ vibrational vector and computing transition dipolar moment $\boldsymbol{\mu}_{\mathbf{ij}}$ induced in the distorted configuration with the use of TD-DFT. HT vibronic intensity is proportional to the squared $\boldsymbol{\mu}_{\mathbf{ij}}$.

Franck-Condon (FC) and Jahn-Teller (JT) activity was modeled using the method reported by Negri *et al.*[30] Namely, if no normal mode rotation and frequency change in the excited states are assumed, vibronic activity of ith vibrational mode in the S_j excited state is determined by displacement parameter B_{ij},

$$B_{ij} = 0.172\omega_i^{0.5}\mathbf{\Delta X_{0,j}}\mathbf{M^{0.5}}\mathbf{L_i}, \quad (1)$$

where ω_i is the frequency of the ith vibrational mode, $\mathbf{\Delta X_{0,j}}$ is the vector defying the change in the Cartesian coordinates between the ground and S_j excited states, $\mathbf{M}$ is diagonal matrix of atomic masses, and $\mathbf{L_i}$ is vibrational eigenvector (in mass-weight Cartesian coordinates). Thus, modeling FC and JT activity requires geometry optimization for the excited states which meets severe difficulties for polyatomic molecules due to high computational demands and, more importantly, root flipping problem. Namely, while optimization of the geometry parameters of the first excited states was successfully fulfilled for $C_{60}F_{18}$, it was found impractical for C_{60} due to the high density of electronic states in the range of the lowest energy electronic transitions. A simplified approach proposed in Ref. 30 and tested in this work for C_{60} was to evaluate B_{ij} from the single-point computations of the excited state gradients at the ground-state geometry,

$$B_{ij} = 2.41 \times 10^6\omega_i^{-1.5}\mathbf{E_j'}\mathbf{M^{-0.5}}\mathbf{L_i}, \quad (2)$$

where $\mathbf{E_j'}$ is the gradient of the excited state S_j computed at the S_0 geometry. Intensity of a nth member of progression in the ith mode is defined by the equation,

$$I_{ij}(n)/I_{0,j} = (\gamma_i)^n/n\,!\,, \quad (3)$$

where $I_{0,j}$ is intensity of the pure electronic transition or HT false origin, while γ_{ij} is,

$$\gamma_{ij} = 0.5B_{ij}^2. \quad (4)$$

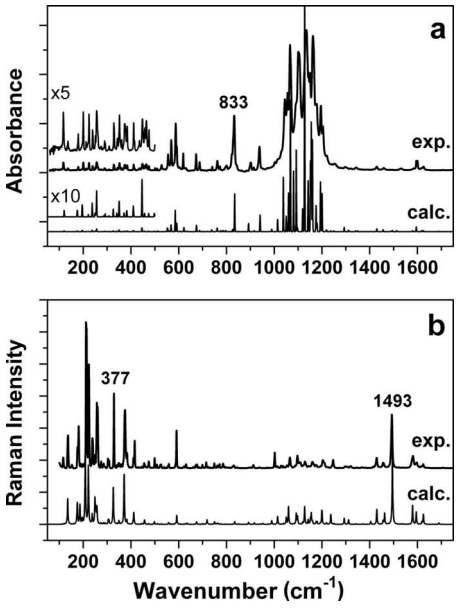

FIG. 2. (a) IR and (b) Raman spectra of $C_{60}F_{18}$ powder: experimental (upper curves) and computed (lower curves).

IV. RESULTS AND DISCUSSION

A. Vibrational spectra

Experimental IR and Raman spectra of the powder $C_{60}F_{18}$ are compared to the calculated spectra in Fig. 2. C_{3v}-symmetric $C_{60}F_{18}$ molecule has 117 IR and Raman active vibrations $(41A_1+76E)$ and such a high number of allowed vibrations inevitably results in rather complicated spectra. Nevertheless, theoretical computations provide almost peak-to-peak agreement with the measured data and enable us to propose tentative assignment of the spectra (a more detailed analysis of the vibrational spectra will be reported elsewhere). Significantly, such a good agreement points to the reliability of the computed vibrational eigenvectors and justifies their use in further calculations of vibronic intensities (see below).

As in the other fluorofullerenes,[28,31,32] IR spectrum of $C_{60}F_{18}$ is dominated by a group of strong absorptions in the 1000–1250 cm^{-1} range, which are assigned to the C–F stretching vibrations partially mixed with the C(F)–C(F) stretching. Strong absorptions are also observed at 833 cm^{-1} and in the 550–600 cm^{-1} range. The line at 833 cm^{-1} is assigned to the complex A_1-symmetric vibration with the comparable contributions from C–C stretch and C–F bend, while the groups of lines at 550–600 cm^{-1} are due to CCC deformations, especially those in the fluorinated belt of the molecule. A lot of weak far-IR bands are due to the carbon cage vibrations mixed with the CCF angle deformations.

Raman spectrum of $C_{60}F_{18}$ has the strongest lines at 200–300 cm^{-1}, a group of medium-to-strong lines in the 300–500 cm^{-1} range, several weak bands in the 1000–1300 cm^{-1} range, a strong line at 1493 cm^{-1}, and weaker features around 1600–1620 cm^{-1}. C–F stretching vibrations have low Raman intensity, while the spectrum is dominated by the low-frequency radial cage modes analogous to the squashing cage mode of C_{60} $[H_g(1)$ at 270 $cm^{-1}]$

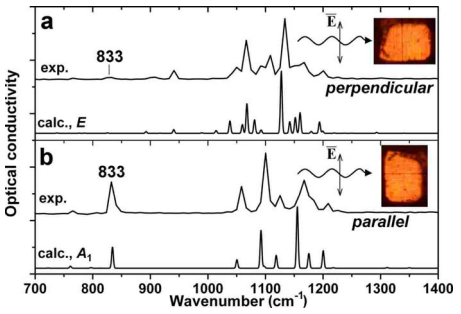

FIG. 3. (Color online) Experimental polarized conductivity spectra measured in (a) perpendicular and (b) parallel orientations of the polarization plane of the incident light with respect to the longer side of the crystal face as compared to the DFT-calculated IR spectra [(a) only E modes and (b) only A_1 modes].

mixed with the CCF deformations. A strong line at 377 cm^{-1} has a significant contribution of the breathing cage mode, while stand-alone medium intensity line at 1493 cm^{-1} is assigned to the pentagon pinch mode in the bare fullerenelike hemisphere similar to the $A_g(2)$ mode of C_{60}.

Availability of the high-quality single crystal of $C_{60}F_{18}$ for reflectance measurements enabled us to study polarization dependence of the IR spectra. Rotation of the polarization vector of the incident radiation resulted in the substantial difference in the optical conductivity in the IR range. Figure 3 shows the spectra measured in two different orientations with respect to vector $\bar{E}$ of linear-polarized incident light, referred hereafter to as parallel and perpendicular, which exhibited the most pronounced differences. For example, the band at 833 cm^{-1} is one of the most intense bands in the parallel orientation but it is almost absent for the perpendicular orientation; other intense bands are observed at 763, 1058, 1100, 1126, 1167, and 1209 cm^{-1} for parallel orientation and at 941, 1050, 1067, 1092, 1109, 1134, 1167, and 1201 cm^{-1} in perpendicular orientation. The spectra for all other orientations did not show any new bands and could be modeled by a superposition of the spectra shown in Fig. 3. Pronounced differences in the spectra measured with two perpendicular orientations of the polarization plane may help in evaluation of the orientations of the individual fluorofullerene molecules with respect to the crystal face. IR active vibrations of $C_{60}F_{18}$ are transformed as A_1 and E symmetry types. In the totally symmetric A_1 modes, dipolar momentum vector oscillates along the C_3 symmetry axis of the molecule, while E modes correspond to the oscillations in the plane perpendicular to the symmetry axis. Figure 3 compares components of the DFT computed spectra, corresponding to A_1 and E modes. As can be seen, A_1-symmetry vibrations are in perfect agreement with the spectrum measured in parallel orientation, while E-symmetry modes match the spectrum measured for the perpendicular orientation. Thus, based on the polarized IR spectra and DFT calculations one may conclude that $C_{60}F_{18}$ molecules are oriented so that their symmetry axis is aligned parallel to the crystal face and along its longer side [Fig. 1(b)]. However, some misalignment of the molecules in the lattice is possible since, for example, A_1-symmetry mode at 833 cm^{-1} is not completely vanished in the perpendicular orientation of the polarization vector.

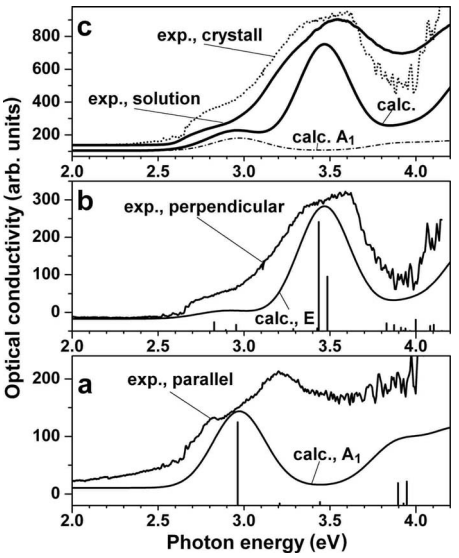

FIG. 4. (a) Optical conductivity in parallel orientation; calculated spectrum shows only $S_0 \rightarrow n\ ^1A_1$ excitations. (b) Optical conductivity in perpendicular orientation; calculated spectrum shows only $S_0 \rightarrow n\ ^1E$ excitations. (c) Superposition of optical conductivity in parallel and perpendicular orientations with the weight factor 2 for the latter (dotted line) and the spectrum of $C_{60}F_{18}$ measured in toluene solution (solid line). Calculated spectrum (dashed line) and $S_0 \rightarrow n\ ^1A_1$ contributions (thin dashed-dotted line) are shown for comparison. For the sake of comparison, calculated spectra in (a)–(c) are broadened with Gaussian peaks (half with 0.2 eV) and shifted in the energy scale by 0.36 eV.

This observation is in line with the x-ray single-crystal structure of $C_{60}F_{18}$, in which symmetry axes of individual $C_{60}F_{18}$ molecules are not exactly parallel to each other with the maximum misalignment angle reaching 26°.[14]

B. Optical spectra in the visible range

The optical conductivity spectra of the single crystal in the visible and UV ranges measured for parallel and perpendicular orientations are shown in Figs. 4(a) and 4(b). Selection rules for the electron excitation are the same as in the IR spectra, hence the optical conductivity spectra for the parallel and perpendicular orientations of the crystal correspond to $S_0 \rightarrow n\ ^1A_1$ and $S_0 \rightarrow n\ ^1E$ excitations, respectively. In Fig. 4(c), superposition of the single-crystal spectra is compared to the absorption spectrum of the toluene solution of $C_{60}F_{18}$ in the same energy range. Optical conductivity spectra of the crystalline fluorofullerene correspond well to the solution spectrum thus showing that intermolecular interactions do not play significant role in the optical conductivity of the material in the visible range and that the spectra may be conceived as originating from the noninteracting individual molecules. Likewise, the onset at 2.57 eV (toluene solution) and 2.64 eV (single crystal) may be assigned to the lowest energy excitation in the individual $C_{60}F_{18}$ molecules. The band-gap value of $C_{60}F_{18}$ is significantly higher than that of C_{60} (1.9 eV) which may be explained by substantial reduction in the fullerene π system in this fluorofullerene.

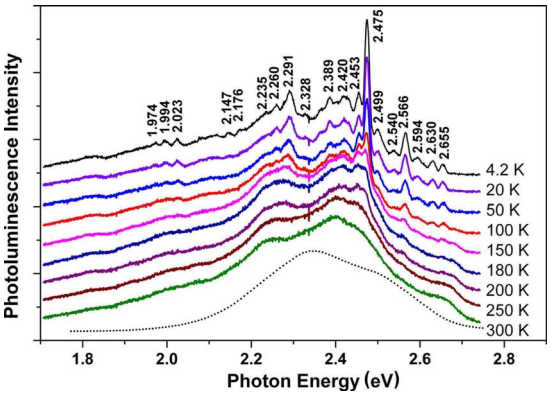

FIG. 5. (Color online) Photoluminescence spectra of toluene solution (300 K, dotted line) and variable-temperature spectra of single crystal.

Optical conductivity for the perpendicular orientation is noticeably lower than for the parallel orientation. Taking into account the weight factor of 2 applied in the superposition due to the twofold degeneracy of E states, one may conclude that transitions to the ^1E excited states are dominating in the unpolarized absorption spectra of $C_{60}F_{18}$. Thus, polarized optical conductivity spectra for the parallel orientation provide unique information about excitation to $^1A_1$-symmetry states, which are otherwise masked by much more intense $S_0 \rightarrow n\ ^1E$ transitions.

Room temperature photoluminescence spectra of $C_{60}F_{18}$ in the crystalline state and in the toluene solution show a broad band peaked around 2.4 eV with the features at 2.66, 2.40, and 2.24 eV (crystal) and 2.51 and 2.35 eV (toluene solution) (Fig. 5). The spectrum of the solution did not show noticeable changes in the spectral pattern over the 430–530 nm (2.88–2.34 eV) excitation wavelengths. The onset observed at 2.7 eV in both spectra confirms the value of the band gap as 2.6 eV evaluated from the absorption spectra, and partial overlap of the absorption and emission spectra may be ascribed to the anti-Stokes components of the vibrational structure of $S_0 \leftrightarrow S_1$ transitions. Upon lowering the temperature, the spectrum of the crystalline $C_{60}F_{18}$ exhibited drastic line narrowing, and fine vibronic structure developed starting from 150 down to 4.2 K (Fig. 4), though still superimposed on the broad-band background. Interestingly, the highest energy line at 2.655 eV, which is assigned to the pure electronic transition (0-0 hereafter), has low intensity compared to other vibronic lines. If $S_0 \leftrightarrow S_1$ transition is dipole allowed, this may suggest strong Franck-Condon activity, that is, significant changes in the molecular geometry in the first excited state. Alternatively, such a vibronic pattern may be explained by the dipole-forbidden 0-0 transition and vibronic activations of $S_0 \leftrightarrow S_1$ transition by the Herzberg-Teller mechanism.

C. Time-dependent DFT calculations and assignment of the spectra

As in the parent fullerene, excitations of $C_{60}F_{18}$ in the visible and near-UV range may be ascribed to π-π^* transitions. To get a deeper insight into the nature of electron excitations in $C_{60}F_{18}$, we have computed electronic structure, excitation energies, and oscillator strengths of $C_{60}F_{18}$ molecule by TD-DFT (see Table I). DFT calculations of the ground state have shown that the frontier molecular orbitals of $C_{60}F_{18}$ are localized presumably on the bare fullerenelike fragment of the molecule [for instance, both highest occupied molecular orbital (HOMO) and lowest unoccupied molecular orbital (LUMO)] and on the benzene ring (for instance, LUMO+2). HOMO and LUMO of $C_{60}F_{18}$ both have E symmetry (see Fig. 6 for the symmetry and energy of MO levels), and hence HOMO→LUMO excitations result in A_1+A_2+E excited states. Of these, the lowest energy is predicted for the dipole-forbidden $^1A_2$ state (see discussion below).

In Fig. 4 experimental optical conductivity spectra are compared to the calculated spectra for the $S_0 \rightarrow n\ ^1A_1$ excitations [Fig. 4(a)], $S_0 \rightarrow n\ ^1E$ excitations [Fig. 3(b)], and overall spectrum [Fig. 4(c)]. Since TD-DFT systematically underestimates excitation energies in fullerenes (for instance, an underestimation by 0.3–0.4 eV were reported by Bauernschmitt *et al.*[33]), computed spectra were upshifted in the energy scale by 0.36 eV for a better comparison to the experimental data. As can be seen, results of TD-DFT calculations are in reasonable agreement with the experimental spectra, especially for the $S_0 \rightarrow n\ ^1E$ excitations, and the strong band at 3.5 eV is readily assigned to the quasidegenerated $S_0 \rightarrow 6\ ^1E$ and $S_0 \rightarrow 7\ ^1E$ excitations. The energy of the $S_0 \rightarrow 1\ ^1A_1$ excitation is still significantly underestimated, but assignment of this transition to the band at 3.2 eV is unambiguous as there are no other intense excitations of A_1 symmetry expected in this energy range. For a better understanding of the nature of the most intense transitions, we have visualized their difference electron density (that is, the difference of the electron density of the excited state and the ground state) on Fig. 7. $S_0 \rightarrow 1\ ^1A_1$ excitation is mainly localized on the nonfluorinated half of the molecule, while in $S_0 \rightarrow 6\ ^1E$ and $S_0 \rightarrow 7\ ^1E$ excitations the electron is promoted from the fullerenelike fragment of $C_{60}F_{18}$ to the π^* orbitals of benzene ring. The major configuration describing transition to $1\ ^1A_1$ state is HOMO→LUMO (92%), while transitions to $6\ ^1E$ and $7\ ^1E$ states are more complex with the largest contributions found for HOMO−2→LUMO (57% and 20%, respectively) and HOMO−1→LUMO+2 (27% and 70%, respectively) (Table I).

Let us now turn to the interpretation of the photoluminescence spectra of $C_{60}F_{18}$ shown in Fig. 5. As the lowest energy excitation of $C_{60}F_{18}$ is assigned to the optically forbidden $S_0 \rightarrow 1\ ^1A_2$ transition, PL spectra of $C_{60}F_{18}$ should be interpreted as a system of vibronic transitions from $^1A_2$ state activated via HT mechanism. However, only HT activity is not sufficient to explain vibronic pattern of $C_{60}F_{18}$ as the experimental spectrum is extended for at least 5500 cm^{-1} (0.68 eV) from 0-0 origin, while intramolecular vibrations of $C_{60}F_{18}$ span the range of 100–1700 cm^{-1} (Fig. 2). Thus, Franck-Condon progressions of HT false origins should be taken into account as well. This situation is reminiscent of C_{60}, whose HOMO-LUMO excitations are also dipole forbidden, and transitions to and from these states are activated by HT mechanism.[34] Likewise, PL spectrum of C_{60} crystals shows similar temperature behavior as found for $C_{60}F_{18}$, with

TABLE I. Lowest energy excited states of $C_{60}F_{18}$ (with major configurations) as predicted by TD-DFT.

$S_0 \rightarrow S_n$	E (eV)	Shifted E (eV)[a]	f	Leading configuration (%)[b]
$S_0 \rightarrow 1\ ^1A_2$	2.455	2.815	0.0000	HOMO→LUMO (73), HOMO−1→LUMO+1 (21)
$S_0 \rightarrow 1\ ^1E$	2.466	2.826	0.0071	HOMO→LUMO (66), HOMO→LUMO+1 (30)
$S_0 \rightarrow 2\ ^1A_2$	2.507	2.867	0.0000	HOMO−1→LUMO+1 (78), HOMO→LUMO (21)
$S_0 \rightarrow 2\ ^1E$	2.534	2.894	0.0008	HOMO−1→LUMO (51), HOMO→LUMO+1 (28), HOMO→LUMO (18)
$S_0 \rightarrow 3\ ^1E$	2.594	2.954	0.0051	HOMO−1→LUMO (46), HOMO→LUMO+1 (34), HOMO→LUMO (14)
$S_0 \rightarrow 1\ ^1A_1$	2.603	2.963	0.0167	HOMO→LUMO (92)
$S_0 \rightarrow 2\ ^1A_1$	2.847	3.207	0.0004	HOMO−2→LUMO (97)
$S_0 \rightarrow 3\ ^1A_2$	2.909	3.269	0.0000	HOMO−2→LUMO (97)
$S_0 \rightarrow 4\ ^1E$	2.926	3.286	0.0017	HOMO−2→LUMO+1 (94)
$S_0 \rightarrow 4\ ^1A_2$	3.057	3.417	0.0000	HOMO→LUMO+2 (100)
$S_0 \rightarrow 5\ ^1E$	3.066	3.426	0.0022	HOMO→LUMO(+2) (98)
$S_0 \rightarrow 6\ ^1E$	3.075	3.435	0.0877	HOMO−2→LUMO (57), HOMO−1→LUMO+2 (27)
$S_0 \rightarrow 3\ ^1A_1$	3.082	3.442	0.0007	HOMO→LUMO+2 (97)
$S_0 \rightarrow 7\ ^1E$	3.125	3.485	0.0437	HOMO−1→LUMO+2 (70), HOMO−2→LUMO (20)

[a]Calculated excitation energies shifted to the higher energy by 0.36 eV for a better comparison to experimental data.

[b]Contributions of less than 10% are omitted.

fine vibronic structure developed at low temperatures.[35,36] Fine structure of the vibronic emission spectrum of C_{60} was also studied in the inert gas matrices,[37] and its theoretical interpretation was given based on CNDO/S calculations.[34,38]

To get further theoretical support for the proposed interpretation of the low-temperature PL spectrum of $C_{60}F_{18}$, vibronic intensities were computed with the use of TD-DFT. Group theory analysis shows that excitation to the A_2-symmetry states can be activated via A_2 and E normal modes. HT intensity of a given normal mode was estimated by distorting DFT-optimized ground-state molecule geometry along this normal coordinate and calculating induced transition moment by TD-DFT. These calculations have shown that HT activity of A_2-symmetric modes is very low compared to that of E modes. The highest HT activity was predicted for the E mode at 1462 cm^{-1} (in the ground-state vibrational spectra of $C_{60}F_{18}$ this mode is assigned to the weak Raman band at 1456 cm^{-1}). Table II lists all vibrations of $C_{60}F_{18}$ which HT activity exceeds 10% of the activity of

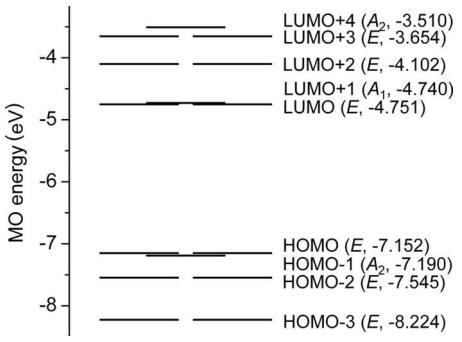

FIG. 6. MO energy levels and orbital symmetries in $C_{60}F_{18}$ molecule in the range of frontier orbitals as predicted by DFT.

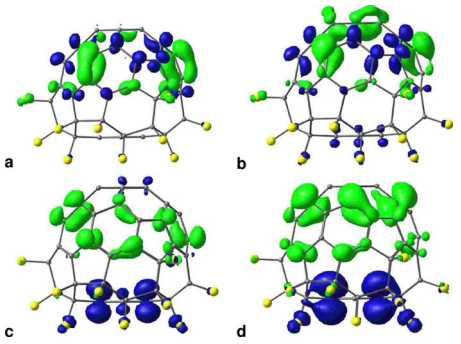

FIG. 7. (Color online) Difference electronic densities for the excitations: (a) $S_0 \rightarrow 1\ ^1A_2$, (b) $S_0 \rightarrow 1\ ^1A_1$, (c) $S_0 \rightarrow 6\ ^1E$, and (c) $S_0 \rightarrow 7\ ^1E$. Blue (dark) lobes correspond to the positive value of difference density, green (light) lobes—to the negative difference density.

TABLE II. Calculated vibrational frequencies (ν), HT intensity (I_{HT}), and relative IR and Raman intensities ($I_{IR,\ Raman}$) of *E*-symmetry modes of $C_{60}F_{18}$ with high HT activity ($I_{HT} > 10\%$) and corresponding bands in the experimental PL, IR, and Raman spectra.

Calc.				Expt.				
ν (cm^{-1})	I_{HT} (%)	I_{IR} (%)	I_{Raman} (%)	PL band	ν_{IR} (cm^{-1})	I_{IR}	ν_{Raman} (cm^{-1})	I_{Raman}
172.9	36.7	0.02	3.40	*A*				
175.3	21.5	0.24	25.78	*A*	179	***w***	177	***m***, ***sh***
186.3	18.3	0.01	23.67	*A*			181	***s***
208.6	34.3	0.00	100.00	*A*	212	***vw***	212	***vs***
237.8	10.6	0.50	11.79	*A*	240	***w***	239	***m***
358.9	12.7	0.00	0.34		362	***vw***	360	***vw***
409.6	23.3	0.39	2.35	*B*	411	***w***	411	***w***
446.0	21.5	1.36	0.97	*B*	448	***m***	447	***vw***
474.1	20.6	0.13	0.73	*B*	475	***w***	475	***w***
511.9	40.5	0.20	0.88	*B*	510	***w***	509	***vw***
526.9	28.2	0.01	0.53	*B*			522	***vw***
552.7	16.5	1.28	0.04	*B*	555	***m***	554	***vw***
567.8	11.3	2.45	0.53	*B*	569	***s***		
621.6	27.7	1.49	0.29	*C*	619	***m***		
635.3	26.5	0.14	1.55	*C*	633	***w***	631	***w***
687.4	32.3	0.41	0.25	*C*	688	***m***	685	***vw***
699.3	65.4	0.06	0.85	*C*			699	***vw***
718.4	36.6	0.02	5.45	*C*			715	***vw***
738.2	15.3	0.64	0.30	*C*	741	***w***		
749.8	10.1	0.01	3.09	*C*			749	***vw***
758.7	36.5	0.17	0.70	*C*				
776.3	20.3	0.34	0.71	*C*	772	***w***	771	***vw***
850.3	10.3	0.05	0.57				843	***vw***
916.7	33.3	0.31	1.82	*D*	914	***w***	913	***vw***
1014.2	11.6	4.42	9.75				1012	***vw***
1092.4	52.4	5.39	2.57		1107		1105	***w***
1142.2	12.3	18.87	5.45		1149	***vs***		
1160.1	15.8	33.26	3.33	*E*	1162	***vvs***	1166	***sh***
1193.8	24.6	18.33	1.19	*E*	1196	***s***		
1199.5	22.2	3.52	10.87	*E*				
1219.6	12.5	0.54	1.38	*E*				
1237.1	24.5	0.25	11.95	*E*			1247	***w***
1250.3	11.2	0.28	1.03	*E*	1260	***vw***		
1293.1	14.4	1.52	7.41		1296	***w***	1298	***vw***
1341.2	24.1	0.29	0.68	*F*	1343	***w***	1345	***vw***
1371.3	35.9	0.01	0.60	*F*			1367	***vw***
1392.6	22.9	0.00	0.08	*F*			1378	***vw***
1455.9	70.9	0.65	4.21	*F*	1459	***w***		
1462.3	100.0	0.00	13.66	*F*			1456	***w***
1532.8	60.0	0.01	0.30	*G*				
1579.6	29.6	0.33	23.29	*G*	1584	***w***, ***sh***	1581	***w***
1594.9	15.7	1.67	15.15	*G*	1598	***m***	1597	***w***
1689.5	15.3	0.06	1.61	*G*	1702	***w***	1708	***vw***

TABLE III. CC bond lengths (Å) in $C_{60}F_{18}$ in the ground and the first excited state.

	Expt.	Calc.			
	X ray	S_0 [a]	S_1 [b]	S_1' [b]	S_1'' [b]
a	1.375	1.382	1.381	1.383	
b	1.382	1.380	1.381	1.378	
c	1.484	1.483	1.482	1.481	1.482
d	1.634	1.639	1.639	1.640	1.637
e	1.562	1.569	1.568	1.567	1.569
f	1.544	1.578	1.578	1.578	
g	1.682	1.688	1.687	1.691	
h	1.528	1.527	1.527	1.532	1.528
i	1.485	1.507	1.506	1.505	1.506
j	1.368	1.373	1.369	1.401	1.375
k	1.421	1.440	1.446	1.415	1.436
l	1.430	1.433	1.439	1.412	1.431
m	1.372	1.400	1.414	1.403	
n	1.451	1.443	1.419	1.453	
o	1.387	1.398	1.420	1.414	1.395
p	1.439	1.438	1.412	1.460	1.437
q	1.454	1.453	1.462	1.421	1.458
r	1.396	1.403	1.387	1.429	
s	1.453	1.447	1.464	1.424	

[a]DFT-optimized bond lengths in ground state (C_{3v} symmetry).
[b]S_1, S_1', and S_1'' denote DFT optimized bond lengths in the first singlet excited state (C_s symmetry). S_1' and S_1'' mark columns with the bonds marked by one and two primes in Fig. 6. (e.g., c', c'', etc). In the ground state all three types of bonds (e.g., **c**, **c**′, and **c**″) are equivalent.

1462 cm^{-1} mode along with the list of corresponding features observed in the ground-state IR and Raman spectra.

FC activity of the totally symmetric modes was estimated by calculating the scalar multiplication of the normal mode vector and the vector, defining the change in the atomic coordinates upon excitation of the molecule [Eq. (1)]. Thus, analysis of the FC activity required optimization of the $C_{60}F_{18}$ geometry parameters in $^1A_2$ excited state, which was also fulfilled with the use of TD-DFT. Table III compares optimized bond lengths of $C_{60}F_{18}$ in the ground and excited states, while Schlegel diagram of $C_{60}F_{18}$ with notation of C–C bonds is shown in Fig. 8. In the ground state, $C_{60}F_{18}$ has C_{3v} molecular symmetry and DFT-predicted interatomic distances agree with the available single-crystal x-ray diffraction data.[14] In the excited state, the symmetry of the molecule is reduced to C_s. While fluorinated half of the molecule retains its geometric parameters in the excited state, the bare fullerenelike part of $C_{60}F_{18}$ molecule exhibits noticeable changes in the interatomic distances. For instance, the changes in the bond lengths of $C_{60}F_{18}$ in the excited state compared to the bond lengths in the ground state reach 0.032 Å. Moreover, in C_s-symmetric 1 $^1A_2$ excited state the alteration of the bond lengths, which are equivalent in C_{3v}-symmetric ground state, can be as high as 0.04 Å (Table III). However, these changes are still comparably small, resulting in the low FC activity. The γ values of the vast majority of $C_{60}F_{18}$ vibrational modes are less than 0.10 [note that γ determines intensity ratio of the false-origin and the first member of its FC progression; see Eq. (4)], and only two vibrations of the molecule has their γ values exceeding 0.10, namely, A_1 modes with DFT-calculated frequency of 120 cm^{-1} (γ=0.12) and 1495 cm^{-1} (γ=0.24). The list of totally symmetric vibrational modes of $C_{60}F_{18}$ with $\gamma > 0.01$ is given in Table IV.

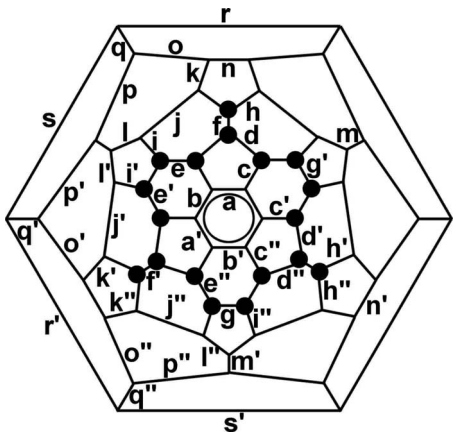

FIG. 8. Schlegel diagram of $C_{60}F_{18}$ with notation of the bonds. The bonds labeled by the same letter with different number of primes (e.g., c, c', and c'') are equivalent in the ground state (C_{3v} symmetry) but become different in the first excited state (C_s symmetry).

TABLE IV. Calculated vibrational frequencies (ν), γ values and relative IR, and Raman intensities ($I_{\mathrm{IR,\ Raman}}$) of A_1-symmetry modes of $C_{60}F_{18}$ with noticeable FC activity ($\gamma > 0.01$) and corresponding bands in the experimental IR and Raman spectra.

Calc.				Expt.			
ν (cm^{-1})	γ	I_{IR} (%)	I_{Raman} (%)	ν_{IR} (cm^{-1})	I_{IR}	ν_{Raman} (cm^{-1})	I_{Raman}
119.7	0.12	0.24	0.74	117	*w*	116	*w*
249.3	0.10	0.14	29.89	251	*vw*, *sh*	257	*s*
255.7	0.03	0.93	4.64	256	*w*	260	*s*, *br*
326.2	0.03	0.03	44.07			329	*s*
411.4	0.09	0.07	13.88			415	*m*
456.2	0.10	0.07	3.68	459	*w*	455	*w*
497.6	0.04	0.13	3.10	500	*w*	499	*w*
1155.3	0.02	40.40	13.32	1162	*vvs*	1160	*w*
1429.8	0.02	1.02	18.68	1430	*w*	1429	*w*
1489.6	0.04	0.16	1.42				
1495.1	0.24	0.40	94.29	1496	*vw*	1493	*s*
1624.8	0.02	0.31	12.31	1626	*w*	1624	*w*

In summary, TD-DFT predicts that luminescence spectrum of $C_{60}F_{18}$ is dominated by HT false origins, while FC progressions are limited to their second members. Figure 9(b) shows that the computed spectrum provides a good match to the low-temperature experimental data, however, FC activity is somewhat underestimated by theory. Note that lowering of the molecular symmetry in the $1\ ^1A_2$ excited state suggests that 0-0 transition should actually become weakly allowed and is indeed observed as a low-intensity feature at 2.655 eV. Due to the comparably low molecular symmetry of $C_{60}F_{18}$, it is hardly possible to interpret experimentally observed peaks in the PL spectra as originating from some specific vibronic transitions of $C_{60}F_{18}$. Rather, each band in the experimental spectrum is the result of the overlap of several FT false origins and their FC progressions. The tentative assignment of the prominent experimental bands [labeled as **A**–**G** in Fig. 9(b)] to *E*-symmetry vibrations of $C_{60}F_{18}$ is given in Table II. For the two strongest PL bands **C** and **F**, shifted from the 0-0 transition by 715 and 1450 cm^{-1} (2.566 and 2.475 eV in the absolute scale, respectively) the first members of FC progressions based on the totally symmetric mode at 1495 cm^{-1} can be clearly identified as the bands marked **C**′ and **F**′ in Fig. 9(b).

It is instructive to compare vibronic spectrum of $C_{60}F_{18}$ to vibronically resolved PL spectrum of C_{60} measured in Ne matrix[37] and for the single crystal[39] to the spectra computed in this work for both molecules with the use TD-DFT (Fig. 9). Modeling of the fluorescence spectrum of C_{60} is additionally complicated by the quasidegeneracy of its three lowest excited states ($1\ ^1G_g$, $1\ ^1F_{1g}$, $1\ ^1F_{2g}$), all comparably contributing to the spectrum. Thus, in our calculations we suggested that the lowest energy state is $1\ ^1F_{1g}$ followed by $1\ ^1F_{2g}$ and $1\ ^1G_g$ with the energy difference of 10 and 50 cm^{-1} following their assignment by Orlandi *et al.*[34] TD-DFT calculations also reproduce the quasidegeneracy of these three states,[40] but as correct energy difference between the state is crucial for reasonable modeling of the experimental spectra, we preferred to use experimentally determined values from Ref. 34 in the modeling. Note also that due to the quasidegeneracy of these states, optimization of their geometry parameters by TD-DFT appears impossible at this moment, and in the com-

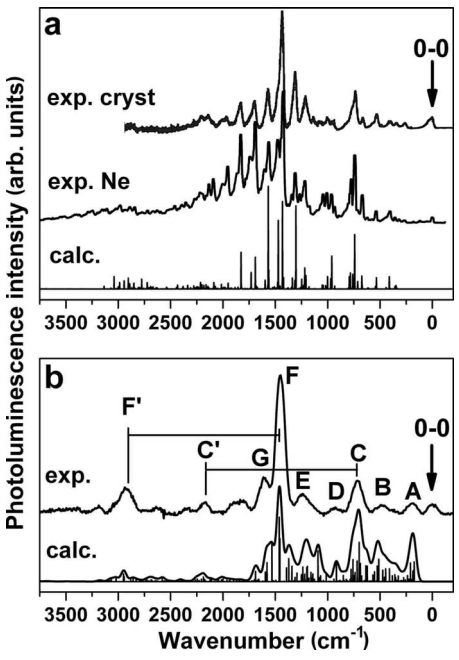

FIG. 9. (a) Experimental PL spectrum of crystalline C_{60} at 4 K from Ref. 39 and of C_{60} in Ne matrix at 4 K from Ref. 33 and TD-DFT calculated spectrum. In calculated PL spectra of C_{60}, zero corresponds to the energy of $1\ ^1G_g$ state, while 0-0 origins of $1\ ^1T_g$ and $1\ ^1T_{2g}$ are assumed to be 10 and 40 cm^{-1} lower in energy (Ref. 30). (b) Experimental (single crystal, 4 K) and calculated PL spectra of $C_{60}F_{18}$. Broadband background in the experimental spectrum is subtracted for clarity. Calculated spectra are broadened with Gaussian peaks (half with 0.2 eV).

putation of FC and JT intensities we used simplified scheme based on the calculations of the gradients of the excited states in the ground-state geometry [Eq. (2)]. Just like for the fluorofullerene, computed spectrum of C_{60} reasonably matches experimental data. To our knowledge, all calculations of the vibronic structure of fullerene and its derivatives reported before were performed by semiempirical methods. Results of our work demonstrate that TD-DFT method, even when such a simple assumption as Eq. (2) is made, provides good agreement to the experimental data and hence can be used for detailed understanding of electronic excitation processes in fullerenes and their derivatives as was already demonstrated for medium-size molecules.[41]

Compared to the fluorescence spectrum of $C_{60}F_{18}$, the spectrum of C_{60} is better resolved, but overall similarity with the data for the fluorofullerene is clear: the most intense bands in both spectra are found around 700–750 and 1400–1450 cm^{-1}. The spectra demonstrate similar degree of FC (and JT for C_{60}) activity, which is manifested in the comparable extension of the spectra beyond the range of the normal intramolecular modes of C_{60} and $C_{60}F_{18}$. The lines around 700–750 cm^{-1} are assigned to radial vibrations of C_{60} or nonfluorinated part of $C_{60}F_{18}$ molecule, while the lines near 1400–1450 cm^{-1} are presumably due to C=C stretching vibrations of C_{60} and $C_{60}F_{18}$. Likewise, in both molecules the highest FC activity is predicted for the pentagon pinch mode, which in C_{60} occurs at 1465 cm^{-1} $[A_g(2)]$, while in $C_{60}F_{18}$ its frequency is upshifted to 1493 cm^{-1} (note that for both molecules the theory somewhat underestimates FC activity).

V. CONCLUSIONS

This work reports an in-depth analysis of the lowest energy excitations of the fluorofullerene $C_{60}F_{18}$ by the use of comprehensive experimental and theoretical methods, including but not limiting to the measurements of polarized optical conductivity of $C_{60}F_{18}$ single crystal in the IR and visible-ultraviolet range, variable-temperature photoluminescence spectroscopy in the 4–300 K, and time-dependent DFT calculations. Analysis of the experimental data combined with calculations can be summarized as follows.

A combination of polarized optical conductivity of $C_{60}F_{18}$ single crystal in the IR range with vibrational DFT calculations enabled us to determine orientation of the individual $C_{60}F_{18}$ molecules with respect to the crystal plane used in present measurements. $C_{60}F_{18}$ molecules are oriented so that their C_{3v}-symmetry axes (corresponding to orientation of electrical dipole moment) are aligned parallel to plane, which is thus shown to be [101]. However, some misalignment of molecules in the lattice is possible since the modes of A_1 symmetry, which should be active only in the parallel orientation of the polarization vector with respect to the molecular axes, do not completely vanished for the perpendicular orientation. This agrees with the earlier single-crystal x-ray diffractions study of solvent-free $C_{60}F_{18}$.[14]

$S_0 \rightarrow n\ ^1E$ electronic excitations are shown to be more intense than the $S_0 \rightarrow n\ ^1A_1$ excitations. Normally, the latter could not be observed experimentally by conventional spectroscopic techniques, being masked by the $S_0 \rightarrow n\ ^1E$ transitions, and only the use the single-crystal polarized measurements made the present observations possible. Both polarized UV-vis optical conductivity and PL spectra of the $C_{60}F_{18}$ single crystal have shown the band gap of 2.6 eV. PL data and TD-DFT calculations have demonstrated that the lowest excited state of $C_{60}F_{18}$ at 2.64 eV has the A_2 symmetry, and therefore a pure electronic $S_0 \rightarrow S_1$ excitation is dipole forbidden. However, vibronic structure of a $S_1 \rightarrow S_0$ transition can be activated via Herzberg-Teller and Franck-Condon mechanisms, and fine vibronic structure was observed at low temperatures in the luminescence spectrum of $C_{60}F_{18}$ single crystal.

Low temperature experimental and calculated vibronic spectra of $C_{60}F_{18}$ single crystals are found to be similar to those of C_{60} molecules in Ne matrix. In both molecules the highest FC activity is predicted for the pentagon pinch mode, which in C_{60} occurs at 1465 cm^{-1} $[A_g(2)]$, while in $C_{60}F_{18}$ its frequency is upshifted to 1493 cm^{-1}. The vibronic structure of the lowest energy excitation of both C_{60} and $C_{60}F_{18}$ is reliably reproduced with the use of TD-DFT calculations, which explain the similar vibronic nature for both molecules by the localization of the lowest energy excitation of $C_{60}F_{18}$ on the nonfluorinated part of the molecule.

To our knowledge, all calculations of the vibronic structure of fullerene and its derivatives reported before were performed by semiempirical methods. Results of this work demonstrate that computations of vibronic structure by TD-DFT method provide a good agreement to the experimental data, and hence this can be used for detailed understanding of electronic excitation processes in fullerenes and their derivatives.

ACKNOWLEDGMENTS

We thank Masaki Tomura (Institute of Molecular Science, Okazaki) for x-ray diffraction measurement and S. I. Troyanov (Moscow State University) for a discussion of the crystalline structure of $C_{60}F_{18}$. Research Computing Center of the Moscow State University is gratefully acknowledged for computer time. We also thank U. Nitzsche for a technical assistance with computer resources in IFW Dresden. This work was supported by CRDF (Award No. RUC2-2830-MO-06 to A.A.P. and O.V.B.), Volkswagen Foundation (Grant I-77/855 O.V.B., A.A.P., I.E.K., and I.V.G.), and Alexander von Humboldt foundation (to A.A.P.).

[1] *Fullerene-Based Materials: Structure and Properties*, edited by K. Prassides (Springer Verlag, Berlin, 2004).
[2] *Carbon Nanotechnology: Recent Developments in Chemistry, Physics, Materials Science and Device Applications*, edited by L. Dai (Elsevier, Amsterdam, 2006).
[3] R. H. Xie, G. W. Bryant, G. Y. Sun, T. Kar, Z. F. Chen, V. H. Smith, Y. Araki, N. Tagmatarchis, H. Shinohara, and O. Ito, Phys. Rev. B **69**, 201403 (2004).
[4] O. Vostrowsky and A. Hirsch, Chem. Rev. (Washington, D.C.) **106**, 5191 (2006).
[5] T. Nakamura, K. Ishikawa, K. Yamamoto, T. Ohana, S. Fujiwara, and Y. Koga, Phys. Chem. Chem. Phys. **1**, 2631 (1999).
[6] J. R. H. Xie, J. J. Zhao, G. Y. Sun, and J. Cioslowski, J. Comput. Theor. Nanosci. **4**, 142 (2007).
[7] R. Hettich, C. M. Jin, and R. Compton, Int. J. Mass Spectrom. Ion Process. **138**, 263 (1994).
[8] O. V. Boltalina and S. H. Strauss, in *Dekker Encyclopedia of Nanoscience and Nanotechnology*, edited by J. A. Schwarz, C. Contescu, and K. Putyera (Dekker, New York, 2004), p. 1175.
[9] A. Gakh, A. A. Tuinman, J. L. Adcock, R. A. Sachleben, and R. N. Compton, J. Am. Chem. Soc. **116**, 819 (1994).
[10] O. V. Boltalina and N. A. Galeva, Usp. Khim. **69**, 661 (2000).
[11] O. V. Boltalina, A. A. Goryunkov, V. Y. Markov, I. N. Ioffe, and L. N. Sidorov, Int. J. Mass Spectrom. **228**, 807 (2003).
[12] O. V. Boltalina, V. Y. Markov, R. Taylor, and M. P. Waugh, Chem. Commun. (Cambridge) 1996, 2549.
[13] I. S. Neretin, K. A. Lyssenko, M. Y. Antipin, Y. L. Slovokhotov, O. V. Boltalina, P. A. Troshin, A. Y. Lukonin, L. N. Sidorov, and R. Taylor, Angew. Chem., Int. Ed. **39**, 3273 (2000).
[14] I. V. Goldt, O. V. Boltalina, L. N. Sidorov, E. Kemnitz, and S. I. Troyanov, Solid State Sci. **4**, 1395 (2002).
[15] S. I. Troyanov, O. V. Boltalina, I. V. Kouvytchko, P. A. Troshin, E. Kemnitz, P. B. Hitchcock, and R. Taylor, Fullerenes, Nanotubes, Carbon Nanostruct. **10**, 243 (2002).
[16] L. G. Bulusheva, A. V. Okotrub, and O. V. Boltalina, J. Phys. Chem. A **103**, 9921 (1999).
[17] R. Mitsumoto, T. Araki, E. Ito, Y. Ouchi, K. Seki, K. Kikuchi, Y. Achiba, H. Kurosaki, T. Sonoda, H. Kobayashi, O. V. Boltalina, V. K. Pavlovich, L. N. Sidorov, Y. Hattori, N. Liu, S. Yajima, S. Kawasaki, F. Okino, and H. Touhara, J. Phys. Chem. A **102**, 552 (1998).
[18] P. V. Dudin, S. V. Amarantov, V. G. Stankevitch, V. N. Bezmelnitsyn, A. V. Ryzkov, O. V. Boltalina, and M. B. Danailov, Surf. Rev. Lett. **9**, 1339 (2002).
[19] A. M. Lebedev, K. A. Menshikov, V. G. Stankevich, N. Y. Svechnikov, A. V. Ryzkov, O. V. Boltalina, I. V. Goldt, I. N. Ioffe, I. A. Kamenskikh, and L. N. Sidorov, Nucl. Instrum. Methods Phys. Res. A **543**, 221 (2005).
[20] V. V. Shnitov, V. M. Mikoushkin, Y. S. Gordeev, O. V. Boltalina, and I. V. Gol'dt, Fullerenes, Nanotubes, Carbon Nanostruct. **14**, 297 (2006).
[21] A. M. Lebedev, K. A. Menshikov, N. Y. Svechnikov, V. G. Stankevich, O. V. Boltalina, I. V. Goldt, S. Kimura, T. Nishi, I. Akimoto, and K. Kan'no, Nucl. Instrum. Methods Phys. Res. A **575**, 96 (2007).
[22] A. M. Lebedev, K. A. Menshikov, V. G. Stankevich, N. Y. Svechnikov, A. A. Popov, O. V. Boltalina, O. Drozdova, and S. Kimura, Diamond Relat. Mater. **16**, 1236 (2007).
[23] D. N. Laikov, Chem. Phys. Lett. **281**, 151 (1997).
[24] D. N. Laikov and Y. A. Ustynuk, Russ. Chem. Bull. **54**, 820 (2005).
[25] J. P. Perdew, K. Burke, and M. Ernzerhof, Phys. Rev. Lett. **77**, 3865 (1996).
[26] A. A. Granovsky, PC GAMESS version 7.1, http://classic.chem.msu.su/gran/gamess/index.html
[27] A. A. Popov, A. A. Goryunkov, I. V. Goldt, I. E. Kareev, I. V. Kuvychko, W. D. Hunnius, K. Seppelt, S. H. Strauss, and O. V. Boltalina, J. Phys. Chem. A **108**, 11449 (2004).
[28] A. A. Popov, V. M. Senyavin, O. V. Boltalina, K. Seppelt, J. Spandl, C. S. Feigerle, and R. N. Compton, J. Phys. Chem. A **110**, 8645 (2006).
[29] P. Pulay, G. Fogarasi, G. Pongor, J. E. Boggs, and A. Vargha, J. Am. Chem. Soc. **105**, 7037 (1983).
[30] F. Negri, G. Orlandi, F. Zerbetto, and M. Z. Zgierski, J. Chem. Phys. **103**, 5911 (1995).
[31] J. V. Rau, S. N. Cesaro, O. V. Boltalina, V. Agafonov, A. A. Popov, and L. N. Sidorov, Vib. Spectrosc. **34**, 137 (2004).
[32] N. I. Denisenko, S. I. Troyanov, A. A. Popov, I. V. Kuvychko, B. Zemva, E. Kemnitz, S. H. Strauss, and O. V. Boltalina, J. Am. Chem. Soc. **126**, 1618 (2004).
[33] R. Bauernschmitt, R. Ahlrichs, F. H. Hennrich, and M. M. Kappes, J. Am. Chem. Soc. **120**, 5052 (1998).
[34] G. Orlandi and F. Negri, Photochem. Photobiol. Sci. **1**, 289 (2002).
[35] D. J. Vandenheuvel, G. J. B. Vandenberg, E. J. J. Groenen, J. Schmidt, I. Holleman, and G. Meijer, J. Phys. Chem. **99**, 11644 (1995).
[36] V. Capozzi, M. Santoro, G. Celentano, H. Berger, and G. F. Lorusso, J. Lumin. **76**, 395 (1998).
[37] A. Sassara, G. Zerza, and M. Chergui, J. Phys. B **29**, 4997 (1996).
[38] A. Sassara, G. Zerza, M. Chergui, F. Negri, and G. Orlandi, J. Chem. Phys. **107**, 8731 (1997).
[39] I. Akimoto and K. Kan'no, J. Phys. Soc. Jpn. **71**, 630 (2002).
[40] A. A. Popov, V. M. Senyavin, and S. I. Troyanov, J. Phys. Chem. A **110**, 7414 (2006).
[41] M. Dierksen and S. Grimme, J. Chem. Phys. **120**, 3544 (2004).